JACS
JOURNAL OF THE AMERICAN CHEMICAL SOCIETY

Article

pubs.acs.org/JACS

Complete Series of {FeNO}^{8}, {FeNO}^{7}, and {FeNO}^{6} Complexes Stabilized by a Tetracarbene Macrocycle

Claudia Kupper,[†] Julian A. Rees,[‡,§] Sebastian Dechert,[†] Serena DeBeer,*[,‡,∥] and Franc Meyer*[,†]

[†]Institut für Anorganische Chemie, Georg-August-Universität, Tammannstrasse 4, D-37077 Göttingen, Germany
[‡]Max Planck Institute for Chemical Energy Conversion, Stiftstrasse 34-36, D-45470 Mülheim an der Ruhr, Germany
[§]Department of Chemistry, University of Washington, Box 351700, Seattle, Washington 98195-1700, United States
[∥]Department of Chemistry and Biochemistry, Cornell University, Ithaca, New York 14853, United States

Supporting Information

ABSTRACT: Use of a macrocyclic tetracarbene ligand, which is topologically reminiscent of tetrapyrrole macrocycles though electronically distinct, has allowed for the isolation, X-ray crystallographic characterization and comprehensive spectroscopic investigation of a complete set of {FeNO}^{x} complexes (x = 6, 7, 8). Electrochemical reduction, or chemical reduction with $CoCp_2$, of the {FeNO}^{7} complex **1** leads to the organometallic {FeNO}^{8} species **2**. Its crystallographic structure determination is the first for a nonheme iron nitroxyl {FeNO}^{8} and has allowed to identify structural trends among the series of {FeNO}^{x} complexes. Combined experimental data including ^{57}Fe Mössbauer, IR, UV−vis−NIR, NMR and Kβ X-ray emission spectroscopies in concert with DFT calculations suggest a largely metal centered reduction of **1** to form the low spin (S = 0) {FeNO}^{8} species **2**. The very strong σ-donor character of the tetracarbene ligand imparts unusual properties and spectroscopic signatures such as low ^{57}Fe Mössbauer isomer shifts and linear Fe−N−O units with high IR stretching frequencies for the NO ligand. The observed metal-centered reduction leads to distinct reactivity patterns of the {FeNO}^{8} species. In contrast to literature reported {FeNO}^{8} complexes, **2** does not undergo NO protonation under strictly anaerobic conditions. Only in the presence of both dioxygen and protons is rapid and clean oxidation to the {FeNO}^{7} complex **1** observed. While **1** is stable toward dioxygen, its reaction with dioxygen under NO atmosphere forms the {FeNO}^{6}(ONO) complex **3** that features an unusual O-nitrito ligand *trans* to the NO. **3** is a rare example of a nonheme octahedral {FeNO}^{6} complex. Its electrochemical or chemical reduction triggers dissociation of the O-nitrito ligand and sequential formation of the {FeNO}^{7} and {FeNO}^{8} compounds **1** and **2**. A consistent electronic structure picture has been derived for these unique organometallic variants of the key bioinorganic {FeNO}^{x} functional units.

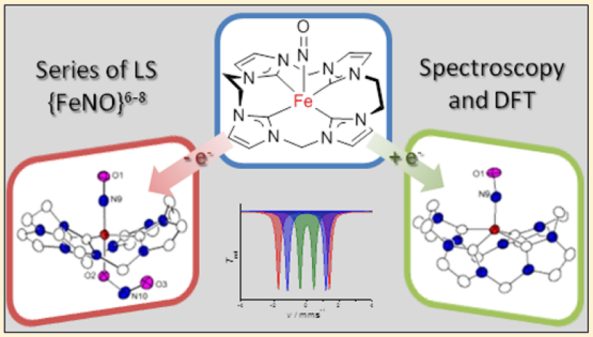

INTRODUCTION

For a long time, nitrogen oxide species (NO_x) were mainly noted for their toxicity and their involvement in air pollution.[1] Meanwhile it is well established that they, and especially nitric oxide (NO) at nanomolar concentrations, play important roles in mammalian physiology such as blood pressure control, neurotransmission, immune response, tissue damage and carcinogenesis.[2,3] Moreover, they are intermediates in the denitrification of nitrate (NO_3^-) to N_2 as part of the biogeochemical nitrogen cycle.[4] The sequential reduction processes of the denitrification pathway are performed by bacterial metalloenzymes, including iron-containing nitric oxide reductases such as rNORs and FNORs.[4] Proposed key intermediates during nitric oxide reduction are iron nitrosyl and nitroxyl complexes, both of the heme and nonheme types.[5]

To understand these fundamental biorelevant NO transformations, model complexes of the types {FeNO}^{8} and [FeNHO]^8, resulting from the reduction of ferrous nitrosyl species {FeNO}^{7} are of particular interest.[6] However, isolation of {FeNO}^{8} species is challenging due to their usually high reactivity and instability. Pioneering spectroelectrochemical studies by Kadish et al. demonstrated a reversible 1-electron reduction of porphyrin-based {FeNO}^{7} complexes,[7] and Ryan et al. investigated the spectroscopic signatures of the {FeNO}^{8} species and their reactivity toward acids and bases.[8,9] The first solid (noncrystalline) material of {FeNO}^{8} porphyrin complexes could be isolated in 2010 by Doctorovich et al.[10] More recently, Lehnert et al. presented characterization and reactivity data for a ferrous heme {FeNO}^{8} including its protonation to [FeNHO]^8,[11] and in 2015 Hu and Li finally succeeded in obtaining single crystals of a heme {FeNO}^{8} that enabled a first X-ray crystallographic structure determination of such a compound.[12] These authors followed the general method of increasing the stability of the iron-nitroxyl by using porphyrins with electron-withdrawing substituents and with a low spin

Received: January 17, 2016
Published: May 18, 2016

DOI: 10.1021/jacs.6b00584
J. Am. Chem. Soc. 2016, 138, 7888−7898

(LS) iron center. Similarly, only few reports on nonheme $\{FeNO\}^8$ compounds can be found in the literature, including Fe-cyclam[13,14] and Fe-TMG_3tren[15] complexes as well as an iron-nitroxyl coordinated by a nonmacrocyclic heme-like 4N-donor ligand,[16,17] or Fe-nitroprusside.[18] Outstanding work on this topic by Wieghardt et al. deserves particular mention, because it disclosed the comprehensive spectroscopic characterization of a complete series of cyclam-based N-ligated $\{FeNO\}^x$ complexes (x = 6, 7, 8) including crystal structures of the $\{FeNO\}^6$ and $\{FeNO\}^7$ compounds.[14] However, crystallographic data for any nonheme $\{FeNO\}^8$ complex is still missing.

Recently, we presented the formation and characterization of an exclusively organometallic $\{FeNO\}^7$ complex (**1**) based on a macrocyclic tetracarbene scaffold, ^{NHC}L.[19] While nonheme iron nitrosyl species, coordinated by N-donors, generally adopt a high spin (HS) state,[20] the tetracarbene ligand ^{NHC}L is an extremely strong σ-donor that leads to a stable LS complex with a linear Fe−N−O moiety. Preliminary electrochemical studies indicated that reversible reduction of the $[^{NHC}L\{FeNO\}^7]^{2+}$ complex **1** is possible, and the resulting $\{FeNO\}^8$ species was identified by in situ Mössbauer and IR spectroscopy.[19,21] Herein, we now report structural parameters obtained by X-ray diffraction as well as a comprehensive spectroscopic characterization and theoretical analysis for the nonheme complex $[^{NHC}L\{FeNO\}^8](OTf)$ (**2**). Furthermore, we present a corresponding oxidized $\{FeNO\}^6$ complex based on ^{NHC}L, which ultimately provides a unique series of structurally characterized organometallic nonheme $\{FeNO\}^x$ complexes (x = 6, 7, 8).

RESULTS AND DISCUSSION

Synthesis. Synthetic transformations reported in this work are summarized in Scheme 1. $[^{NHC}L\{FeNO\}^8](OTf)$(**2**) can be

Scheme 1. Synthetic Transformations of the $^{NHC}L\{FeNO\}^x$ Species (x = 6, 7, 8) Reported in This Work

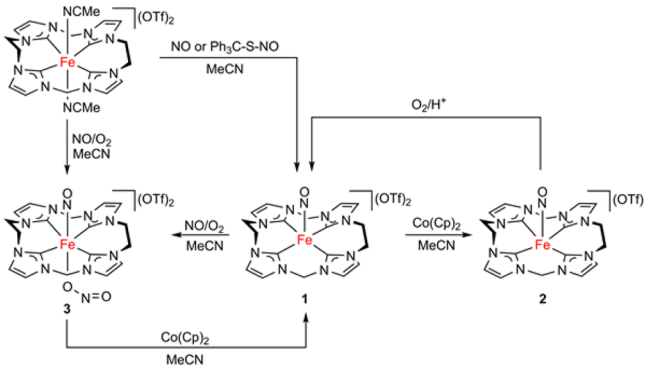

prepared on a preparative scale by reduction of **1** with cobaltocene. To this end, a mixture of **1** and $Co(Cp)_2$ in acetonitrile was reacted in the absence of light at −35 °C, leading to a color change of the solution from blue to green. Addition of diethyl ether (Et_2O) gave a green precipitate of **2** that was washed with Et_2O and hexane (47% yield). Green single crystals suitable for X-ray diffraction were obtained by slow diffusion of Et_2O into an acetonitrile solution of **2** at −35 °C.

Compared to other $\{FeNO\}^8$ compounds, **2** is relatively stable even in solution and could be fully characterized by a bouquet of spectroscopic methods (vide infra). NMR spectroscopy evidences the diamagnetic (LS) character of **2**, and the presence of two doublets for the methylene (CH_2) linkers of the tetracarbene macrocycle at δ = 6.21 and 5.78 ppm ($^2J_{HH}$ = 13.5 Hz) reflects the inequivalence of the two sides of the ^{NHC}LFe plane caused by the apical NO ligand.

The oxidized complex $[^{NHC}L\{FeNO\}^6(ONO)](OTf)_2$ (**3**) containing an O-bound nitrito ligand *trans* to the NO was initially isolated as a side product when **1** was prepared from the precursor complex $[^{NHC}LFe^{II}(MeCN)_2](OTf)_2$[22] and an excess of NO in the presence of trace amounts of O_2. Close examination of the reaction then revealed that **3** is best and reproducibly synthesized in a two-step sequence by first treating an acetonitrile solution of $[^{NHC}LFe^{II}(MeCN)_2](OTf)_2$ with nitric oxide gas, which leads to a color change from yellow to blue indicative of the in situ formation of **1**. Therefore, it is also possible to start directly from the isolated $\{FeNO\}^7$ complex **1**. In the second step, dioxygen is added to the nitric oxide atmosphere, causing the atmosphere to turn brownish immediately and the color of the solution to gradually change to yellow. Yellow crystals of **3** suitable for X-ray diffraction could then be obtained in 63% yield by diffusion of Et_2O into the reaction mixture. **3** proved stable in air for extended periods and was also fully characterized. Similar to compound **2** the NMR spectrum of **3** shows signals in the range typical for a diamagnetic species. Consequently, we can assign all species of this $\{FeNO\}^{6-8}$ series to possess LS ground states. Notably, one of the two doublets for the methylene linkers of the tetracarbene macrocycle (δ = 6.18 and 5.15 ppm; $^2J_{HH}$ = 13.5 Hz) in **3** is significantly shifted upfield compared to **2** and is thus assigned to the proton directed to the side of the ^{NHC}LFe plane where the nitrito-O ligand binds. While the X-band EPR spectrum of **2** is silent as expected, in case of **3** we observed less than 5% of a paramagnetic species (see Figures S13 and S14). Wieghardt et al. suggested that trace amounts of the corresponding $\{FeNO\}^7$ species might be responsible for the EPR signal often observed for $\{FeNO\}^6$ complexes.[23] However, in the present case the signal shows great similarity with the EPR signature of a related LS ferric complex $[^{NHC}LFe^{III}(MeCN)_2]^{3+}$ with axial acetonitrile ligands; we thus assume that in solution some NO is released and replaced by a MeCN solvent molecule.

In the literature, different possibilities have been considered for the formation of a coordinated nitrite when reacting iron complexes with an excess of NO. In 1984, Yoshimura et al. reported that the reaction of nitrosyl porphyrinato iron(II) complexes with excess nitric oxide gas leads to compounds $[Fe(porph)(NO)(NO_2)]$,[24] which they explained by a disproportionation reaction between coordinated NO with 3 equiv of free NO to form the coordinated ligands $(NO)(NO_2)$ and free N_2O. A similar mechanism was later found by Lippard et al. for an iron tropocoronand system and supported by in situ IR spectroscopy.[25] However, in the present case we did not observe any evidence for such a mechanism because **1** is stable in the presence of excess NO, and the conversion to **3** starts only after addition of dioxygen. A possible scenario involving dioxygen could be the direct reaction of coordinated NO with O_2 to give the iron nitrito complex,[26] but we consider this scenario unlikely for two reasons. First, the coordination mode of the resulting NO_2 ligand would likely be N-bound nitro. Second, no NO_2 ligand formation is observed upon treating **1** with O_2 in the absence of additional nitric oxide gas. In fact, compound **1** is quite stable under dioxygen atmosphere. On the other hand, it is well established and exploited in large scale

DOI: 10.1021/jacs.6b00584
J. Am. Chem. Soc. 2016, 138, 7888−7898

industrial processes that gaseous NO reacts with O_2 to give NO_2 (or its dimer N_2O_4).[27] Nitrogen dioxide (NO_2) can further react with additional NO to give unstable N_2O_3.[28] We thus assume that NO_2 formed in the gas phase undergoes a redox reaction with the starting $\{FeNO\}^7$ complex **1** to finally give the $\{FeNO\}^6(ONO^-)$ product **3**. Lorkovic and Ford reported in 2000 the formation of a related ON-Fe(TPP)-NO_2 heme complex with traces of NO_2, proposing a similar mechanism.[29] To corroborate the suggested transformation, we performed isotope labeling experiments using $^{18}O_2$ which led to the formation of singly and doubly labeled compound **3** as shown by ESI-MS. Since the NO ligand can be released in solution, we also observed the $\{FeN^{18}O\}^6$ compound, according to IR. Still, especially the finding of doubly labeled **3** supports the proposed scenario for the formation of **3** from the reaction of **1** with NO_2. The experiment did not show any significant amounts of labeled product **3** when only one equivalent of $^{18}O_2$ was used even though the reaction proceeded to completion. We assume that the instability of N_2O_x compounds allows for very fast exchange of the oxygen atoms and scrambling with the excess of $N^{16}O$, leading to formation of both, partially labeled NO as well as NO_2 (and hence to singly and doubly labeled compound **3**) with ^{18}O enrichment depending on the amount of $^{18}O_2$ used (see Figure S5 for ESI-MS and Figure S9 for IR data). Further evidence for the proposed mechanism is discussed below within the DFT and reactivity sections.

Crystallographic Details. Both newly synthesized complexes **2** and **3** could be obtained in crystalline form, and their structures were determined by X-ray diffraction. In combination with the recently communicated structure of **1**[19] this constitutes an unprecedented series of tetragonal $\{FeNO\}^{6-8}$ complexes with an identical basal ligand scaffold, allowing for comparison of both structural and spectroscopic trends along the complete series. Molecular structures of the cations of **2** and **3** are depicted in Figure 1, and selected structural parameters

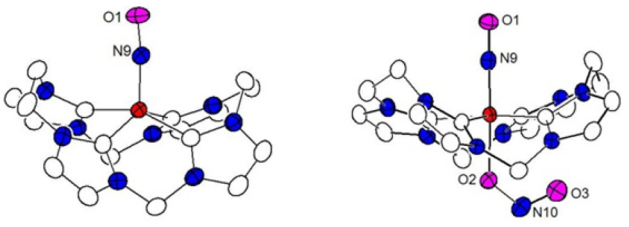

Figure 1. Molecular structures of the cations of **2** (left) and **3** (right) (50% probability thermal ellipsoids); anions and hydrogen atoms have been omitted for clarity.

are collected in Table 1. As in compound **1**, the iron center in **2** is found in roughly square pyramidal (SPY-5) environment, but the iron atom's displacement out of the $\{C_4\}$ basal plane of the ^{NHC}L scaffold toward the apical NO ligand is more pronounced in **2** (0.56 Å compared to 0.41 Å in **1**) which reduces the interaction with the carbene ligand. Increased displacement from the $\{C_4\}$ plane could be due to stronger bonding with the NO as evidenced by the shorter Fe−N9 bond (Table 1). Alternatively, increased repulsion by the carbene could push the Fe up, and a likely redox-active orbital that would explain this is the d_{z^2} with its strongly σ-antibonding torus (see DFT section below). Linearity of the Fe−N9−O1 moiety (176.9° in **1**) is decreased upon reduction to **2** (169.1°), in line with recently published crystallographic data and DFT predictions.[10−12] It

Table 1. Selected Structural Parameters, Bond Lengths [Å] and Angles [°] for 1,[19] 2 and 3

	$\{FeNO\}^6$ **3**	$\{FeNO\}^7$ **1**	$\{FeNO\}^8$ **2**
space group	$P\bar{1}$	$P\bar{1}$	$P2_1/C$
coordination	OC-6	SPY-5	SPY-5
Fe displacement from {C4} plane [Å]	0.12	0.41	0.56
<(Fe−N9−O1) [°]	176.6	176.9	169.1
<(N9−Fe−O2) [°]	175.6	–	–
d(N9−O1) [Å]	1.162	1.166	1.207
d(Fe−N9) [Å]	1.625	1.670	1.660
av. d(Fe−C^{NHC}) [Å]	2.008	1.994	1.968

should be noted though that in those previous examples the Fe−N9−O1 moiety was already bent in the $\{FeNO\}^7$ compound,[12] in contrast to **1**. The N9−O1 distance in **2** is slightly elongated while the Fe−N9 distance is shortened compared to **1**. This trend is explained by addition of one further electron into the SOMO of the $\{FeNO\}^7$ unit that has mainly Fe(d_{z^2}) character (53%) and σ character with respect to the NO moiety (see DFT section below for details). Intuitively one might assume that the addition of an electron would lead to enhanced electronic repulsion between the Fe and the NO ligand and therefore to a longer Fe−NO bond. However, the increased bending within this moiety could reduce this repulsion. Conversely the higher electron density at the Fe center and the increased bending enables better π-backbonding from Fe(d_{xz},d_{yz}) and Fe(d_{z^2}) into the π^*(NO) orbital leading to a shorter Fe−NO bond.

The Fe center in the $\{FeNO\}^6$ compound **3** is coordinated octahedrally (OC-6) with the NO and nitrito-O ligands in the axial positions (angle N9−Fe−O2 175.6°). In this case the Fe atom is displaced only slightly out of the $\{C4\}$ basal plane by 0.12 Å toward the nitric oxide. The Fe−N9−O1 angle is very similar to the one in complex **1** (176.6°) while both the N9−O1 and the Fe−N9 distances are slightly shorter. The distance between the Fe and the O-bound nitrito ligand, d(Fe−O2), is 1.98 Å and therefore much longer than the distance between the Fe and the NO, indicating a stronger bonding of the latter ligand. The N−O bonds within the nitrito ligand are also much longer than the one in the NO ligand (FeO2−N10O3 1.31 Å and FeO2N10−O3 1.20 Å), as expected. Even though many reports of oxidized nonheme $\{FeNO\}^6$ ferric nitrosyls are found in the literature,[30] few octahedral compounds have been isolated so far.[31,13] Furthermore, analysis of changes in properties during both reduction and oxidation of a particular $\{FeNO\}^7$ complex is rather limited since full characterization of the related $\{FeNO\}^8$ species are usually lacking. Interestingly, in complex **3** an O-bound nitrito ligand is found, contrasting the predominant N-nitrito (nitro) coordination.[30] Some compounds with nitrosyl and N-nitrito ligands *trans* to each other are found in the literature.[23,24,32] To the best of our knowledge, only Wieghardt et al. in their comprehensive study reported a comparable O-nitrito $\{FeNO\}^6$ complex.[13,14]

Spectroscopic Characterization. Zero-field ^{57}Fe Mössbauer spectra and characteristic Mössbauer parameters of complexes **1**−**3** are presented in Figure 2 and Table 2. First, we focus on the interpretation of changes in the isomer shift (IS) upon reduction. It should be kept in mind that the IS generally changes as a function of the 4s electron contribution to the electron density at the Fe nucleus and is influenced by several factors; most importantly by the 4s population, the

DOI: 10.1021/jacs.6b00584
J. Am. Chem. Soc. 2016, 138, 7888−7898

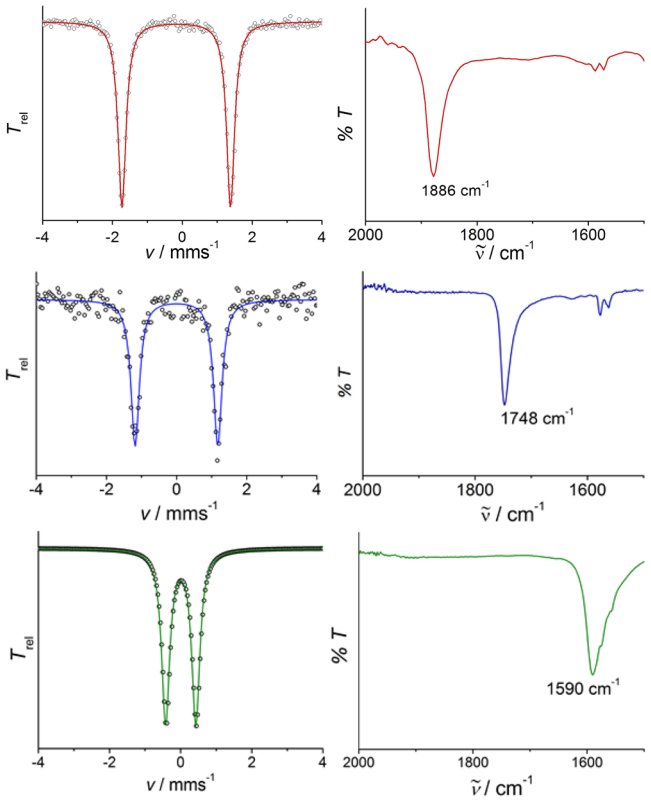

Figure 2. Series of Mössbauer spectra (left) of solid $\{FeNO\}^6$ **3** (top), $\{FeNO\}^7$ **1** (middle)[19] and $\{FeNO\}^8$ **2** (bottom) recorded at 80 K and parts of the ATR-IR spectra (right) of the three complexes.

Table 2. Selected Experimental and DFT Calculated (in Brackets) Spectroscopic Parameters for 1,[19] 2 and 3

	$\{FeNO\}^6$ **3**	$\{FeNO\}^7$ **1**	$\{FeNO\}^8$ **2**
δ [mm s^{-1}]	−0.16 (−0.15)	−0.01 (0.05)	0.02 (−0.05)
ΔE_Q [mm s^{-1}]	3.12 (3.15)	2.36 (2.13)	0.85 (1.37)
ν_{N-O} [cm^{-1}] (solid)	1886 (1887)	1748 (1752)	1590 (1601)
$\nu_{^{14}N-O}$ [cm^{-1}] (MeCN)	1882	1740	1604
$\Delta\nu_{^{14}N-^{15}N}$ [cm^{-1}] (MeCN)	38	32	31

shielding effect due to 3d population, and by the Fe−ligand bond lengths that dictate the radial extension of the 4s wave function.[33,34] For the present system the IS is essentially unchanged upon reduction of **1** (δ = −0.01 mm s^{-1}) to **2** (δ = 0.02 mm s^{-1}). On the basis of these similar IS values for **1** and **2**, a cursory interpretation could indicate a ligand centered reduction as has previously been reported for other LS iron nitroxyl complexes.[20,14] However, the often observed negative correlation of the IS with the oxidation state of the Fe center (with higher oxidation states exhibiting more negative isomer shifts) is mainly valid for high spin compounds or high oxidation states.[33,34]

As IS is a function of s-electron density at the nucleus, the change due to a largely metal-centered reduction, accompanied by enhanced 3d shielding, in the present case is offset by other perturbations upon moving from **1** to **2**. Namely, the shorter Fe−C bonds in **2** lead to a more compressed 4s orbital and therefore higher 4s electron density at the Fe nucleus. Additionally, the slightly contracted Fe−N bond and longer N−O bond in **2** is indicative of increased π-backbonding, effectively depopulating the d orbitals and decreasing the shielding of the 4s from the Fe core. Both of these latter factors would suggest that the IS of **2** should be lower than the IS of **1**. Contrarily, addition of a further electron into the Fe(d_{z^2}) orbital of **1** upon metal-centered reduction (see DFT section) leads to increased shielding of the 3s and 4s electrons, resulting in a higher IS value. Moreover, we find an increased displacement of the Fe from the equatorial ligand plane. The reduced σ-interaction with the macrocyclic tetracarbene results in a lower electron density at the Fe center leading to a higher IS value. Overall these contrary effects can negate each other, leading to the observed negligible changes in IS.

Comparison with recent literature shows that similar effects, where the interplay of different effects led to negligible changes in the IS, were also observed for other low-valent LS complexes such as a number of DNIC compounds.[35] For some iron(IV)alkylidines, unusually high IS values similar to the IS of their iron(II) precursors have been observed, in agreement with similar bond lengths in both species.[36] For a series of Fe−N_2^+, Fe−N_2 and Fe−N_2^- complexes, even a reversed positive correlation of the IS with the Fe oxidation state has been reported.[34,37] Notably, these observations underline that in case of LS-$\{FeNO\}^x$ species the Mössbauer IS cannot be used for a reliable assignment of oxidation states.

In contrast to the IS, the quadrupole splitting (QS) shows a distinct change upon reduction. While the QS in **1** is quite large (ΔE_Q = 2.36 mm s^{-1})—representing the oblate charge distribution around the nucleus—it is found to be strongly decreased in **2** (ΔE_Q = 0.85 mm s^{-1}). In case of the reduced species **2**, the interaction with the tetracarbene ligand is decreased because of the displacement of the Fe out of the ligand plane. This loss of strong equatorial σ-donors decreases the anisotropy at the Fe nucleus. Also, the anisotropy contribution originating from the highly covalent Fe-NO π-backbonding interaction is expected to be perturbed upon addition of a further electron. These changes are nicely reflected in the distinct decrease in QS upon reduction from **1** to **2**.

The $\{FeNO\}^6$ compound shows a very low IS at δ = −0.16 mm s^{-1}, perfectly in line with the Fe atom being located much more in the plane of the four equatorial NHC donors compared to **1** and **2**. Interestingly, this IS value is even more negative than the one observed for the oxoiron(IV) complex $[^{NHC}LFe^{IV}=O]^{2+}$ (δ = −0.13 mm s^{-1}).[22] For a related $\{FeNO\}^x$ series, Wieghardt et al. interpreted the oxidation as well as the reduction of a cyclam-based $\{FeNO\}^7$ complex to occur largely at the ligand.[14] However, **3** is formed by reaction of a NO_2 radical with the $\{FeNO\}^7$ species, and NO_2 is clearly reduced to NO_2^- while the oxidation occurs largely metal centered (vide infra). In essence, upon oxidation the 3d electron density at the Fe center is reduced and the 4s electrons become less shielded. Again, this is in agreement with the very low IS. Moreover, as typically observed for iron complexes with the macrocyclic tetracarbene ligand ^{NHC}L, **3** shows a very large quadrupole splitting ΔE_Q = 3.12 mm s^{-1}, which is the result of extensive charge donation into the Fe $3d_{x^2-y^2}$ orbital giving an oblate charge distribution around the Fe nucleus.[38]

In the IR spectra the ν_{NO} stretching frequency for solid $\{FeNO\}^8$ **2** was found at 1590 cm^{-1} (1604 cm^{-1} in acetonitrile solution; Figures 2 and S8, Table 2), in line with the longer N−O bond compared to the precursor complex **1** (ν_{NO} at 1748 cm^{-1}). Overall, stretching frequencies for **1** and **2** are relatively

DOI: 10.1021/jacs.6b00584
J. Am. Chem. Soc. 2016, 138, 7888−7898

high and in the range known for HS complexes rather than LS complexes, likely due to the unusual linearity of the Fe−N−O moiety.[19,20] The shift of 158 cm^{-1} upon reduction from **1** to **2** can originate from either ligand or metal centered reduction: addition of one electron into the π^*(NO) orbital would weaken the N−O bond, whereas reduction of Fe would lead to increased π−backbonding. In view of the combined structural and theoretical analysis (vide infra) we assume this reduction to occur largely metal centered. In line with the shorter N−O bond in **3**, ν_{NO} is shifted by 140 cm^{-1} to higher wavenumbers (solid: 1886 cm^{-1}; acetonitrile solution: 1882 cm^{-1}) upon oxidation of **1** to the {FeNO}^{6} complex. Labeling with ^{18}O gives rise to a new signal at 1841 cm^{-1} (acetonitrile solution), most likely the ν_{NO} stretch in ^{18}ON−Fe−ONO (Figure S9). Unfortunately, even with the help of DFT calculations the stretching frequencies of the nitrito moiety could not be unambiguously assigned. Superimposed solid state spectra of ^{16}O- and ^{18}O-labeled species are given in the SI (Figure S9). A labeling experiment with ^{15}NO led to the expected shift of the ν_{NO} stretching frequencies to lower energy by 31−38 cm^{-1} (Table 2; and see SI).

The Fe → NHC charge transfer (CT) band in the UV−vis−NIR spectrum of **2** (λ_{max} 360 nm; Figure S6, S21) is more intense and red-shifted compared to the one of **1** (λ_{max} 350 nm) in line with higher electron density at the Fe center. Moreover, the broad Fe → NO transition at 615 nm in {FeNO}^{7} **1**[19] is shifted to 642 nm in the case of {FeNO}^{8} **2** while the intensity is slightly decreased. This band represents the lowest energy HOMO → LUMO transition and the shift to lower energies agrees well with the HOMO−LUMO gap being slightly smaller in **2** compared to **1**, in accordance with DFT results (vide infra, Figures S21 and S22). Interestingly, a similar transition within the Fe-NO moiety is completely missing for {FeNO}^{6} **3**, which is lacking any characteristic transition beyond 450 nm; only a broad band at 306 nm with a shoulder around 380 nm was found in the UV−vis spectrum of **3** (Figure S6). These transitions were assigned to be mainly Fe−ONO and Fe−NO related (Figures S21, S23, and S24).

Complexes **1**−**3** as well as the iron(II) precursor [^{NHC}LFe^{II}(MeCN)$_2$](OTf)$_2$ were further characterized by Kβ X-ray emission spectroscopy (XES). The Kβ mainline region, corresponding to Fe 3p to 1s transitions, is a sensitive probe of metal-centered spin density.[39] The absence of low-energy shoulders (Kβ' features) in the mainlines of **1**−**3** is consistent with a low-spin state in all of the complexes (Figure S12). Transitions in the higher energy valence-to-core (VtC) region originate from orbitals that are dominantly ligand in character, and can be understood using molecular orbital theory.[40] The dipole-allowed intensity depends on metal p mixing into the donor orbitals, and thus only ligand orbitals that interact with the metal in a σ fashion give rise to spectral features. Additionally, both the energies and intensities of most spectral features are accurately calculated using a one-electron DFT approach.[40,41]

The VtC region is comprised of higher-energy K$\beta_{2,5}$ features, the result of transitions originating from ligand p-type orbitals, and lower-energy Kβ'' features, which are primarily due to ligand s-type orbitals. With this in mind, tentative assignment of the spectral features shown in Figure 3 can be made for **1**−**3** and for the iron(II) precursor [^{NHC}LFe^{II}(MeCN)$_2$](OTf)$_2$. All four spectra possess an intense K$\beta_{2,5}$ peak in the ∼7106−7108 eV region, which may be attributed to the tetracarbene macrocycle given the σ-donating nature of the ligand and its

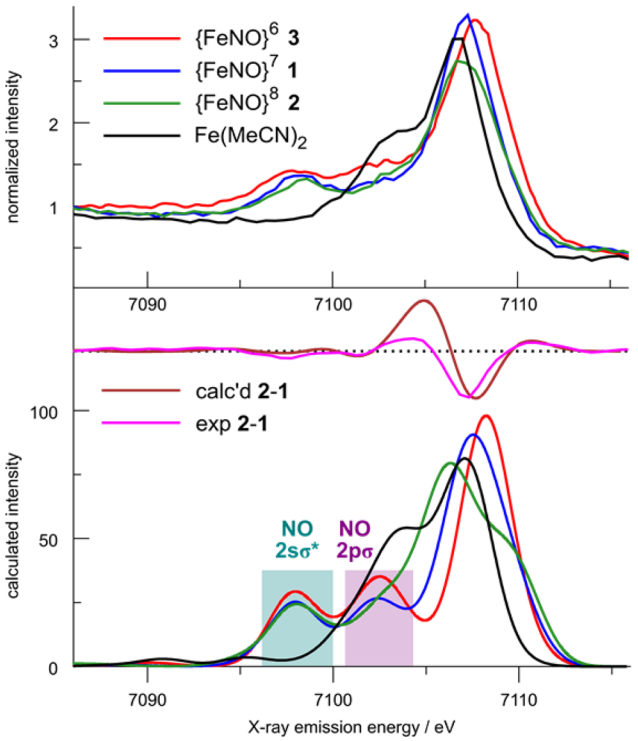

Figure 3. Top: Fe Kβ VtC XES spectra of **1**−**3** and the iron(II) precursor [^{NHC}LFe^{II}(MeCN)$_2$](OTf)$_2$. The Kβ'' feature at ∼7098 eV is assigned as transitions from NO 2sσ*, and the difference (**2**−**1**) highlights the spectral changes upon reduction of **1**. Bottom: DFT-calculated VtC XES spectra of **1**−**3** and the iron(II) precursor [^{NHC}LFe^{II}(MeCN)$_2$](OTf)$_2$. The difference trace highlights the successful calculation of subtle differences between the spectra of **1** and **2**. A 55.6 eV shift was used to correct the calculated transition energies, and a 3 eV broadening was applied to the combined transition moments.[39]

presence in the spectrum of the NO-free iron(II) precursor. The precursor spectrum additionally has a pronounced low-energy shoulder, likely from the lone pairs of the axial acetonitriles. The spectra of **1**−**3** all exhibit a much weaker low-energy K$\beta_{2,5}$ shoulder, as well as a Kβ'' peak at ∼7098 eV, which is absent in the precursor spectrum. In light of the highly linear coordination of the NO moiety, the NO 2s$_\sigma$* and the 2p$_\sigma$ molecular orbitals are expected to have optimal σ interaction with the iron. Therefore, we assign these to the low-energy Kβ'' peak and the K$\beta_{2,5}$ shoulder at ∼7102 eV, respectively. This interpretation is consistent with a previous VtC XES study of four-coordinate iron mono- and dinitrosyl complexes by Liaw et al.[42]

We note that in their work, Liaw et al. further proposed that the difference in energy between the NO 2s$_\sigma$*- and the 2p$_\sigma$-derived features could be utilized to quantitatively asses the oxidation state of the NO fragment, a desirable spectroscopic target. However, their calibration of NO oxidation state was performed on an isolated NO molecule, rather than an Fe-NO unit. As Fe−NO complexes are known to have very delocalized bonding orbitals and highly ambiguous redox changes, hence the use of Enemark−Feltham notation, their calibration of an NO fragment has little bearing on intact Fe-NO moieties. Additionally, the intense VtC features they report, that lead to well-resolved spectra, are almost certainly due to the tetrahedral iron geometry, and thus not expected for biologically relevant octahedral and square pyramidal iron nitrosyls. Nonetheless,

DOI: 10.1021/jacs.6b00584
J. Am. Chem. Soc. 2016, 138, 7888−7898

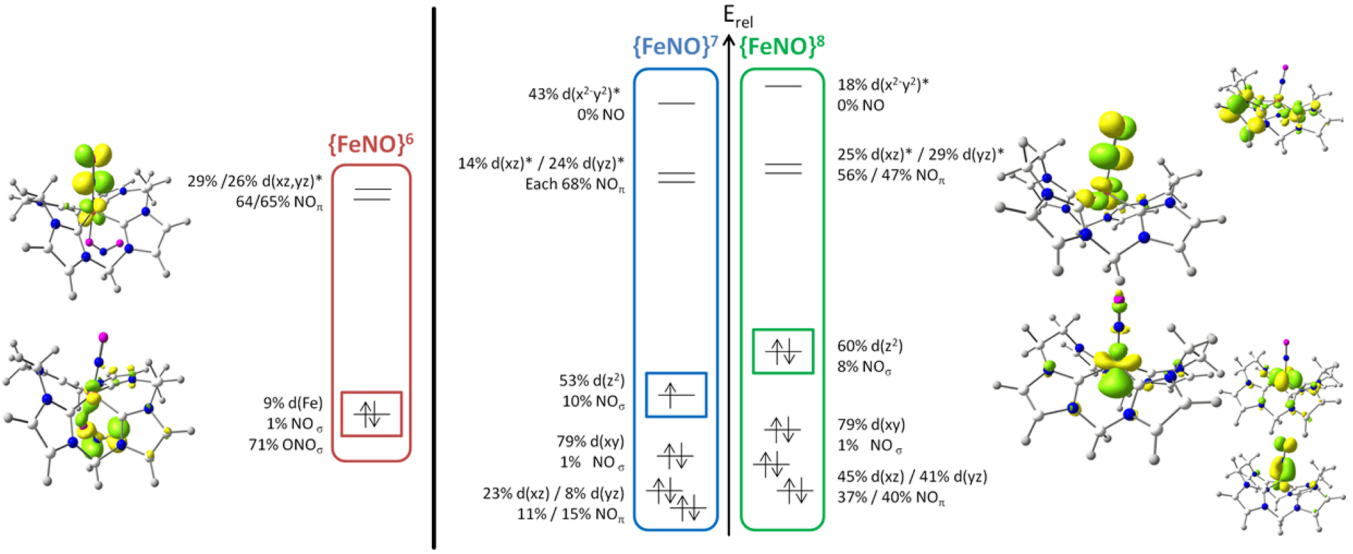

Figure 4. Right: DFT-calculated MO scheme (BP86, def2-tzvp) according to E_{rel} of {FeNO}^{7} **1** (left)[19] and {FeNO}^{8} **2** (right). Values are given for the majority (α) spin orbitals with their dominating iron d-orbital contributions and DFT calculated molecular frontier orbitals of **2** are added on the right side (Counter value 0.06). Left: DFT-calculated HOMO and LUMO of complex **3**.

the splitting of these spectral features, at approximately 7098 and 7103 eV, reflects the energetic difference between NO $2s_\sigma$* and the $2p_\sigma$ orbitals, and provides a qualitative indication of changes to NO oxidation state, particularly within a series of related complexes.

In the present work, we observe negligible changes in the energy difference between these features in the spectra of **1** and **2**. Consistent with our other spectroscopic data (vide supra), this suggests that the reduction of **1** to **2** is mostly metal-centered. Additionally, the VtC features of **1** are largely more intense than **2**. The more acute Fe−N−O angle found in **2** along with further displacement from the tetracarbene plane decreases the amount of σ overlap between metal and ligand orbitals, resulting in weaker spectral features.[43] Similar interpretation of the changes in energies and intensities upon oxidation of **1** to **3** is precluded by coordination of the axial nitrito ligand, which increases the number of donor molecular orbitals in the same energy range. Transitions arising from the nitrito and NO fragments are thus unfortunately experimentally indistinguishable.

DFT Calculations. To gain more insight into the electronic structures of the series of compounds {FeNO}$^{6-8}$ we performed unrestricted DFT calculations. Similar to **1**,[19] the geometries of **2** and **3**, determined crystallographically, could be reproduced well. Important characteristics such as the angles within the Fe−N−O moiety in **2** (exp.: 169.1°, calc.: 174.8°) and **3** (exp.: 176.6°, calc.: 175.3°) agree reasonably well with experimental data. Moreover, calculated Mössbauer parameters (Table 2) reproduce the experiments well, supporting the suitability of the DFT model. In particular, DFT predicts the IS to actually decrease upon reduction from **1** to **2**. Even though DFT slightly overestimates the experimentally observed trend, this is in good agreement with changes in the IS if based on the Fe−NO bond length rather than the oxidation state. Furthermore, we would like to point out that the minor discrepancies between the calculated and experimental MB parameters are within the expected error range (compare Figure S26).[44] Altogether it can be concluded that experiment as well as DFT clearly evidence that the IS of complexes **1** and **2** are essentially identical whereas the QS shows distinct changes upon reduction. Vibrational features in the IR region and UV−vis−NIR transitions could also be calculated with adequate agreement between theory and experiment (see SI for further details). It should be pointed out that the high intensity of the Fe → NHC LMCT transition at 360 nm for complex **2** as well as the lack of any Fe → NO transition for **3** are indeed confirmed by the TD-DFT calculations. Furthermore, DFT predicts Fe−NO stretching frequencies of very low intensity (**2**: T**2 = 1 and **3**: T**2 = 5) and close to intense vibrations within the tetracarbene ligand (T**2 ≈ 90). This is in line with the unsuccessful attempt to assign the Fe-NO stretches upon labeling with ^{15}N. The N−O stretches within the nitrite moiety of the {FeNO}^{6} compound were calculated to 886 cm^{-1} (FeO−NO) and 1502 cm^{-1} (FeON−O) with moderate intensities.

Figure 4 (right) shows the MO scheme of the reduced complex **2** in comparison to the {FeNO}^{7} compound **1**.[19] Upon reduction, the orbital interactions within the valence shell regime undergo only small changes since the energetic order remains unchanged. The HOMO in both species originates from the σ antibonding interaction of the Fe(d_{z^2}) orbital with the NO lone pair. Comparison with {FeNO}^{7} **1** shows that the HOMO of **2** directly derives from the SOMO (α electron) respectively LUMO (β electron) of **1** and shares the main characteristics. In **2** the HOMO has an even higher Fe character (60% Fe(d), 6% N atom of the NO ligand) and a similar admixture of Fe(p_z) character (9%) which clearly is in line with a metal centered reduction. This finding contrasts earlier reports on LS {FeNO}^{8} species for which a SOMO/HOMO with mainly NO character and a largely ligand centered reduction was proposed.[14,12,11,45] However, metal centered reductions were found for the HS species TauD-{FeNO}^{8} and [Fe(TMG$_3$tren)NO]$^+$.[46−48] The LUMO in **1** and **2** originates from the π antibonding combination of the Fe(d_{xz}) orbital (Fe(d) 25%) and the π*(NO) orbital, representing the π-backbonding interaction with a large contribution from the π*(NO) (56%). The corresponding interaction in the *yz*-plane is very close in energy. Furthermore, significant changes within the corresponding bonding interactions between Fe(d_{xz},d_{yz}) and the π*(NO) were observed upon reduction of **1** to give **2**.

DOI: 10.1021/jacs.6b00584
J. Am. Chem. Soc. 2016, 138, 7888−7898

This Fe-NO backbonding interaction (shown at the bottom of the MO scheme) is clearly increased in **2**, and the resulting attenuation of d-orbital population helps to compensate for the addition of the second d_{z^2} electron. Typical for the tetracarbene ligand, the Fe($d_{x^2-y^2}$) orbital is markedly destabilized. For complex **3** only the HOMO and LUMO are shown in Figure 4 (left) because a clean assignment of the calculated interactions to specific Fe(d) orbitals is not possible. Nonetheless, the calculated energetic order of α and β orbitals is presented in Figure S19. Interestingly, the LUMO in {FeNO}^{6} **3** is quite similar (Fe(d) 29%, Fe(s,p) 0%, NO 64%) to the related orbitals of the reduced species **1** and **2**. This finding is clearly in line with a similar π-interaction between the Fe center and the NO ligand in all three species of the present series. However, the HOMO in **3** is mainly located on the O-bound nitrito ligand (71%). Only a minor contribution of the Fe(d) (9%) is found within this bonding σ interaction. This nicely reflects the proposed oxidation of the {FeNO}^{7} moiety upon reaction with NO_2 and is in line with a metal centered oxidation by removal of the unpaired electron from the SOMO of **1** (Fe(d_{z^2})-NO σ-interaction). The electron density is shifted to the nitrite ligand and the iron d_{z^2} orbital, which is left unoccupied in **3**, can thus no longer participate in a bonding interaction between the iron center and the NO ligand. This finding also explains the missing HOMO−LUMO optical transition in **3** compared to **1** and **2**, as the character of the HOMO is completely changed upon oxidation.

The VtC XES spectra were calculated for **1**−**3** and the iron(II) precursor, within a single-electron approximation as described previously.[41] As the calculated spectra are based solely on the ground-state DFT orbitals, comparison to experimental data effectively assesses the quality of the electronic structure description, with regard to both orbital energies and the degree of metal−ligand bonding and metal p−d mixing. As shown in Figure 3, the calculated spectra of all complexes studied have excellent agreement with the experimental data, notably including the presence of a low-energy Kβ'' peak and a K$\beta_{2,5}$ shoulder in the NO-containing complexes and a strong K$\beta_{2,5}$ shoulder in the iron(II) precursor. The difference spectra highlight the successful calculation of subtle differences in electronic structure between **1** and **2**. In the ∼7095−7102 eV region, the negative difference traces reflect more iron p character in the NO ligand orbitals in reduced **2**, and the matching minima indicate that the calculated energy differences between NO $2s_\sigma$* and the $2p_\sigma$ orbitals match the experimental energies. Additionally, the positive feature in both difference spectra at ∼7111 eV indicates an increased transition intensity from the highest-energy donor orbitals, which corresponds to the Fe(d_{z^2}).

To obtain additional insight into the VtC spectra, a fragment analysis was performed with MOAnalyzer.[49] As shown in Figure 5, the Kβ'' and K$\beta_{2,5}$ shoulders correspond to the NO $2s\sigma$* and the $2p\sigma$ molecular orbitals, as expected. Additionally, while the large Kβ2,5 peak is dominantly carbene in character, the high energy shoulder corresponding to the positive difference feature at ∼7111 eV is found to correspond to the Fe(d_{z^2}). The increase in experimental spectral intensity upon reduction to **2** provides strong evidence for a doubly occupied d_{z^2} in **2**, and thus a metal-centered reduction. The high percentage of Fe p_z character found in the d_{z^2} (9%, vide supra) provides a mechanism for spectral intensity, as we have previously observed.[50−52]

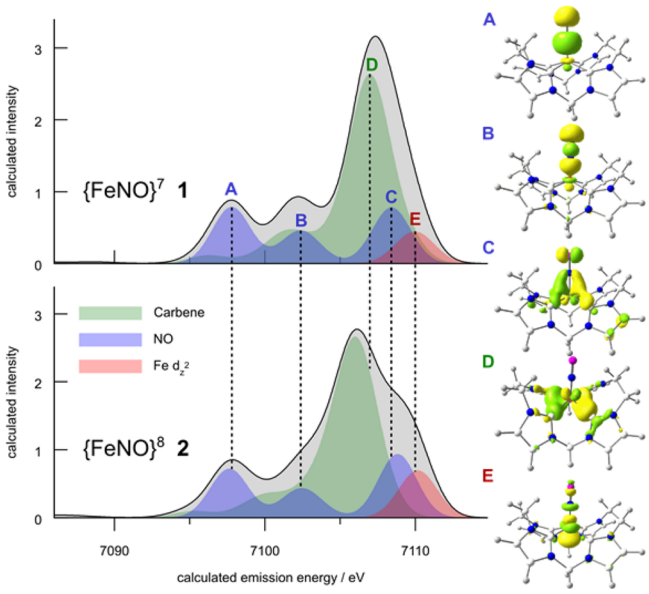

Figure 5. Left: Fragment analysis and spectral deconvolutions of the DFT-calculated VtC XES spectra of **1** (top) and **2** (bottom), showing the contributions to key spectral features. Right: Donor molecular orbitals of **1** corresponding to the most intense transitions at the indicated energies. Importantly, the approximate doubling of the highest-energy d_{z^2} feature upon reduction is due to a second transition of the spin-down electron, indicating a metal-centered reduction.

Reactivity and Redox Properties. Preliminary experiments have been performed to explore the reactivity of these unique organometallic {FeNO}^{x} complexes. Because of its biological relevance, the protonation of {FeNO}^{8} species is of considerable interest. This protonation usually leads to intermediate {FeNHO}^{8} compounds that are in most cases highly unstable and release H_2 via disproportionation, yielding the corresponding {FeNO}^{7} species.[8−11] However, treatment of the tetracarbene coordinated {FeNO}^{8} species **2** with 1,5-bis(dimethyl)piperidinium or 1,5-dimethylpyridinium (pK_a = 14.1)[53] salts under strictly anaerobic conditions led to no reaction according to IR stopped flow measurements. This is in good agreement with a protonation on the nitrogen atom being unfavorable for the present system because the electron density in reduced **2** is located at the Fe instead for the NO. Thus, we find experimental relevance for the metal centered redox processes in the {FeNO}^{x} species described herein as opposed to ligand centered reductions usually described in literature.[11,45] Interestingly, in the presence of dioxygen, protonation of **2** causes an immediate color change from green to blue. Subsequent IR and UV−vis measurements demonstrated complete conversion to the oxidized {FeNO}^{7} species. More specifically, admitting dioxygen to a mixture of **2** and 1 eq of 1,5-bis(dimethyl)piperidinium leads to clean conversion to **1** within five seconds at RT, indicated by three isosbestic points during UV−vis monitoring (Figure S7). This markedly differs from the much slower reaction of {FeNO}^{8} with dioxygen in the absence of acid, where three different isosbestic points are observed (Figure S7) and where the resulting brown suspension contains only small amounts of {FeNO}^{7} but mainly decomposition products of the type $^{NHC}LH_2(NO_x)_2$ and Fe_xO_y, according to mass spectrometry as well as IR and NMR spectroscopies. Hence, we can conclude that only in the presence of protons oxidation of **2** with O_2 leads to clean formation of {FeNO}^{7} and suppression of subsequent

DOI: 10.1021/jacs.6b00584
J. Am. Chem. Soc. 2016, 138, 7888−7898

decomposition processes. This indicates that the $\{FeNO\}^8$ compound can be reoxidized to the corresponding $\{FeNO\}^7$ via a process that involves some coupling of proton and electron transfer (PCET), whereas similar processes have previously been described to occur in a stepwise fashion, namely via initial protonation of the NO moiety followed by an intermolecular redox process. Further studies to elucidate mechanistic details of the PCET-like process are ongoing.

The redox properties of $\{FeNO\}^6$ **3** were also studied, and compared to its reduced analogues. Consistent with the more oxidized nature, the cyclic voltammogram of $\{FeNO\}^6$ **3** in acetonitrile solution shows two redox processes; an irreversible reduction at −0.51 V and a reversible one at −1.00 V vs the Cp_2Fe/Cp_2Fe^+ couple (Figure 6). Interestingly, the latter

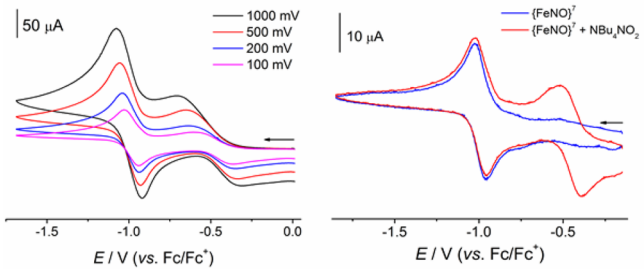

Figure 6. Left: cyclic voltammogram of **3** in MeCN/0.1 M $[Bu_4N]PF_6$ at RT vs Fc/Fc^+ at various scan rates (V = 0.1, 0.2, 0.5, 1.0 V s^{-1}). Right: cyclic voltammograms of **1** (blue) and after addition of 1 equiv $[NBu_4]NO_2$ (red) in MeCN/0.1 M $[Bu_4N]PF_6$ at RT vs Fc/Fc^+ at 50 mV. The red spectrum nicely resembles the CV obtained for compound **3** on the left side.

process closely resembles the reduction observed for **1** to give **2**.[19] In agreement with the electrochemical findings, treatment of $\{FeNO\}^6$(ONO) **3** with one equivalent of cobaltocene on a preparative scale leads to formation of the blue complex **1**, and treatment of **3** with 2 equiv of cobaltocene leads the green complex **2**, according to Scheme 1. As discussed above, the LUMO of **3** has mainly Fe-NO π^* character and therefore a simple reduction is not favored, but is followed by a chemical reaction (EC mechanism). However, instead of the NO the more weakly bound *trans* nitrito ligand is rapidly released, giving the stable $\{FeNO\}^7$ complex **1** that can be reversibly reduced in a subsequent process to the $\{FeNO\}^8$ complex **2**. Reoxidation of **1** at higher potential in the anodic back scan is associated with recoordination of nitrite to give $\{FeNO\}^6$(ONO) **3**.

Additional experiments were performed to support the proposed reaction of $\{FeNO\}^7$ **1** with NO_2 to form $\{FeNO\}^6$(ONO) **3** in a redox process, and the electrochemical interconversion of **3** and **1** in an EC process. Treatment of **1** with nitrite salts ($NaNO_2$ or $[NBu_4]NO_2$) indeed did not lead to any reaction. In the same way, no fast reaction was observed upon treatment of the $\{FeNO\}^7$ complex with a strong oxidant (thianthrenium tetrafluoroborate). This is in accordance with the lack of any oxidation wave in the cyclic voltammogram of **1** up to +1.5 V (vs Fc/Fc^+).[19] However, the combination of both reagents, nitrite and thianthrenium, led to rapid formation of the $\{FeNO\}^6$(ONO) species **3**, according to IR. Still, this reaction is not advantageous compared to the reaction with in situ prepared NO_2 because subsequent decomposition reactions at room temperature were observed. Furthermore, electrochemical experiments in MeCN solution, or in a mixture of MeOH/MeCN, did not show any oxidation of **1** up to +1.5 V vs Fc/Fc^+ (in pure MeOH **1** is poorly soluble).[19] However, when the cyclic voltammogram of **1** in MeCN was measured in the presence of added $[NBu_4]NO_2$, a new quasi-reversible wave appeared (Figure 6, right) which nicely resembles the $\{FeNO\}^6/\{FeNO\}^7$ redox transition observed for compound **3** (Figure 6, left; an additional irreversible oxidation wave at +0.09 V appears after addition of $[NBu_4]NO_2$ and can be assigned to a redox process of the free nitrite salt; see Figure S16). To sum up, all these measurements emphasize that a simple oxidation of **1** to a 5-fold coordinated $\{FeNO\}^6$ species is not possible, but binding of a sixth ligand *trans* to the NO is required. This is in line with conclusions from the spectroscopic and DFT studies that the electron is removed from an orbital having largely Fe(d_{z^2}) character. Furthermore, these redox processes reflect the close relation of the presented series of $\{FeNO\}^x$ complexes, even though $\{FeNO\}^6$(ONO) **3** is not strictly comparable with **1** and **2** due to its 6-fold coordination.

CONCLUSION

We experimentally studied both the reduction and oxidation of the unique $\{FeNO\}^7$ complex **1** featuring equatorial tetracarbene coordination. While ^{NHC}L is topologically related to tetrapyrrole macrocycles, its electronic properties are quite different. Building upon the reversible electrochemical reduction of **1** we succeeded in isolating the organometallic $\{FeNO\}^8$ complex **2**, including its comprehensive spectroscopic and X-ray crystallographic characterization; to our knowledge, this represents the first structure determination of a nonheme $\{FeNO\}^8$ complex. The experimental data, in particular Mössbauer, IR and $K\beta$ XES results, in combination with DFT calculations suggest a largely metal centered reduction of **1** to form the low-spin (S = 0) complex **2**. Due to its extremely strong σ-donor character, the tetracarbene ligand imparts rather unusual properties to **1** and **2** such an almost linear Fe−N−O moiety with high NO stretching frequencies that are in the range of typical high-spin $\{FeNO\}^7$ and $\{FeNO\}^8$ complexes. Minor variations of the Mössbauer IS among the series demonstrate that in case of LS-$\{FeNO\}^x$ species the Mössbauer IS cannot be used for distinct assignment of oxidation states.

Initial reactivity experiments revealed that under strictly anaerobic conditions **2** is not reactive toward acids, which markedly contrasts the protonation of the NO ligand in other $\{FeNO\}^8$ complexes that usually leads to highly unstable $\{FeNHO\}^8$ intermediates; this reflects that the electron density in **2** is largely located on the Fe instead of the NO. Interestingly, only in the presence of both acid and dioxygen is rapid and clean formation of the $\{FeNO\}^7$ species **1** observed, suggesting a PCET-like process for the oxidation.

1 is quite stable in the presence of dioxygen, and the CV of complex **1** in MeCN solution shows no oxidation wave. However, the reaction of **1** with dioxygen under nitric oxide atmosphere leads to formation of the six-coordinate $\{FeNO\}^6$(ONO) complex **3** with an unusual O-nitrito ligand *trans* to the NO. This compound is a new example of the limited number of nonheme octahedral $\{FeNO\}^6$ complexes. Electrochemical and chemical reduction of **3** causes dissociation of the O-nitrito ligand and sequential transformation to the five-coordinate $\{FeNO\}^7$ and $\{FeNO\}^8$ compounds **1** and **2**. These tetracarbene ligated $\{FeNO\}^x$ complexes **1**−**3** thus constitute the first series of Fe-NO complexes for which all three members (x = 6, 7, 8) have been structurally characterized. The findings highlight the ability of NHC ligands to support a range

DOI: 10.1021/jacs.6b00584
J. Am. Chem. Soc. 2016, 138, 7888−7898

of metal oxidation states and to stabilize key bioinorganic functional units, which serves to develop a unified picture of their electronic structures and reactivity patterns spanning biomimetic coordination chemistry and organometallic chemistry.

EXPERIMENTAL SECTION

General Considerations. All reactions were carried out under dry argon using standard Schlenk techniques, or in a glovebox (MBRAUN LabMaster) under dinitrogen atmosphere with less than 0.5 ppm of O_2 and H_2O. Solvents were dried and degassed by standard procedures before use. Chemicals were purchased from commercial sources and used as received. Complex **1**,[19] $[^{NHC}LFe^{II}(MeCN)_2](OTf)_2$[22] as well as 1,5-bis(dimethyl)-piperidinium tetrafluoroborate,[54] 1,5-dimethylpyridinium triflate[53] and thianthrenium tetrafluoroborate[55] were prepared according to literature procedures. Nitric oxide gas was purchased from Linde and passed through a column with Ascarite II and a cooling trap (−78 °C) before being added to the reaction mixture. ^{15}NO gas was prepared in situ by treatment of $Na^{15}NO_2$ with an aqueous solution of ascorbic acid. UV−vis−NIR spectra were collected with a Varian Cary 5000 instrument using quartz cuvettes. Spectra were analyzed by Cary Win UV software. Solid state and solution IR measurements were performed with a Cary 630 FTIR spectrometer with Dial Path Technology and analyzed by FTIR MicroLab software. ESI mass spectra were measured on a Thermo Finnigan Trace LCQ spectrometer. NMR spectra were recorded on Bruker Avance 300 or 500 instruments at 25 °C (**3**) and −35 °C (**2**). Chemical shifts (δ) are given in ppm and are referenced to the solvent residual signals. The peaks are labeled according to their splitting patterns with s (singlet), d (doublet), t (triplet), or m (multiplet). Elemental analyses were performed by the analytical laboratory of the Institute of Inorganic Chemistry at the Georg-August-University Göttingen using an Elementar Vario EL III instrument. Mössbauer (MB) spectra were recorded with a ^{57}Co source in a Rh matrix using an alternating constant-acceleration Wissel Mössbauer spectrometer operated in the transmission mode and equipped with a Janis closed-cycle helium cryostat. Isomer shifts δ are given in mm s^{-1} relative to iron metal at ambient temperature. Simulation of the experimental data was performed with the Mfit program.[56] X-band EPR spectra were measured with a Bruker E500 ELEXSYS spectrometer equipped with a standard cavity (ER4102ST, 9.45 GHz). The sample temperature was maintained constant with an Oxford Instruments Helium flow cryostat (ESP910) and an Oxford temperature controller (ITC-4). The microwave frequency was measured with the built-in frequency counter and the magnetic field was calibrated using an NMR field probe (Bruker ER035M). EPR spectra were simulated using EasySpin.[57] IR Stopped Flow experiments were performed using a T_gK Scientific SF-61/VERTEX 70 IR. The stopped flow machine was controlled with Kineta Drive and the cell was cooled to 5 °C using a cryostat. Data were recorded and analyzed with the OPUS 7.0 program. Cyclic voltammograms were measured using a Perkin Elmer 263 A potentiostat controlled by Powersuite electrochemistry software. A three electrode arrangement with a glassy carbon working electrode, a Ag/0.01 M $AgNO_3$ reference electrode and a Pt wire counter electrode was utilized. All CV experiments were performed under an atmosphere of dry argon in MeCN/0.1 M nBu_4NPF_6. The resulting data were converted to the Fc/Fc^+ scale by using Cp_2Fe, added after the experiment, as internal standard. X-ray emission spectra were collected at beamline C-1 at the Cornell High Energy Synchrotron Source (CHESS, iron(II) precursor, **1**, and **2**) and at beamline ID-26 at the European Synchrotron Radiation Facility (ESRF, iron(II) precursor and **3**). Samples were prepared by grinding neat solid into a fine powder using a mortar and pestle, which was sealed in a 1 mm Al spacer using 38 μm Kapton tape. In both cases, the spectrometers consisted of an array of five Ge(620) analyzer crystals arranged in a Rowland geometry of Johann type, as described previously.[58,41] The spectrometer flight path was filled with helium to mitigate signal attenuation, and samples were maintained below 40 K using a displex (CHESS) or liquid helium flow (ESRF) cryostat. Incident X-ray energies were selected at CHESS and ESRF using a pair of W/B_4C multilayers or a Si(111) double-crystal monochromator, respectively. Analyzed X-ray emission was detected using a Pilatus Si pixel detector or APD. In all cases, samples were screened for radiation damage, and only spectra that exhibited no evidence of photochemistry were averaged to improve the signal-to-noise ratio. Both spectrometers were calibrated to the spectral features of Fe_2O_3,[41] and comparison of the iron(II) precursor spectra recorded on both beamlines confirmed the internal experimental consistency.

Synthesis of $[^{NHC}L\{FeNO\}^8](OTf)$ 2. To a precooled and blue solution of **1** (20.0 mg, 0.027 mmol, 1.00 equiv) in MeCN (2 mL) was added cobaltocene (5.7 mg, 0.030 mmol, 1.1 equiv). The reaction mixture was allowed to react for 3 h at −35 °C under exclusion of light. To the resulting green solution Et_2O (7 mL) was added, causing precipitation of a green solid. The solution was removed via a syringe and the solid was washed with Et_2O (5 mL) and hexane (5 mL) and then dried under reduced pressure to give the crude product (7.5 mg, 0.013 mmol, 47%). Green single crystals suitable for X-ray diffraction were obtained by slow diffusion of Et_2O into a solution of crude **2** in MeCN at −35 °C. ^1H NMR (500 MHz, acetonitrile-d_3) δ 7.49 (s, 4H; CH_{NHC}), 7.29 (s, 4H; CH_{NHC}), 6.21 (d, J = 13.3 Hz, 2H, CH_2), 5.78 (d, J = 13.6 Hz, 2H; CH_2), 4.71 (t, J = 8.6 Hz, 4H; C_2H_4), 4.54−4.27 (m, 4H; C_2H_4).[13] ^{13}C NMR (126 MHz, acetonitrile-d_3) δ 195.85 (C_{NHC}), 125.00 (CH_{NHC}), 123.17 (CH_{NHC}), 62.54 (CH_2), 50.09 (C_2H_4). IR (solid, FTIR): $\tilde{\nu}$ (cm^{-1}) = 3127 (m), 1590 (s), 1464 (s), 1403 (s), 1340 (s), 1259 (m), 1222 (s), 1209 (s), 1153 (s), 1029 (s), 811 (s), 718 (s), 687 (s), 671 (s), 635 (s), 574 (s), 572 (s), 516 (s), 462 (s). UV−vis (solution, MeCN): λ_{max} [nm] (ε [L $mol^{-1}cm^{-1}$]): 300 (6850), 360 (6800), 642 (410).

Synthesis of $[^{NHC}L\{FeNO\}^6(ONO)](OTf)_2$ 3. A yellow solution of $[^{NHC}LFe^{II}(MeCN)_2](OTf)_2$[22] (25 mg, 0.032 mmol) in MeCN (3 mL) in a Schlenk flask wrapped with aluminum foil and closed with a septum was put under slight vacuum and connected to an NO gas source. The gas connection was opened and the solution turned blue within 5 min. Since this color change is attributed to formation of **1**, it is also possible to directly start from the $\{FeNO\}^7$ species at this point. Dry dioxygen was added to the NO gas phase using a syringe (1 equiv or excess). The headspace immediately turned brown indicating the formation of oxidized nitric oxide gases including NO_2, and the solution turned yellow. Yellow single crystals suitable for X-ray diffraction were obtained by diffusion of Et_2O into the reaction mixture at RT (15.0 mg, 0.019 mmol, 63%). ^1H NMR (300 MHz, acetonitrile-d_3) δ 7.61−7.35 (m, 8H; CH_{NHC}), 6.18 (d, J = 13.5 Hz, 2H; CH_2), 5.15 (d, J = 13.5 Hz, 2H; CH_2), 5.05−4.65 (m, 8H; C_2H_4).[13] ^{13}C NMR (75 MHz, acetonitrile-d_3) δ 167.7 (4C, C_{NHC}), 126.1 (4C, CH_{NHC}), 124.3 (4C, CH_{NHC}), 62.2 (4C, CH_2), 49.9 (8C, C_2H_4). IR (solid, FTIR): $\tilde{\nu}$ (cm^{-1}) = 3127 (m), 1877 (s), 1459 (m), 1346 (s), 1257 (m), 1222 (s), 1193 (s), 1140 (m), 1028 (s), 746 (s), 696 (s), 633 (m), 570 (s), 514 (s), 444 (s). UV−vis (solution, MeCN): λ_{max} [nm] (ε [L $mol^{-1}cm^{-1}$]): 306 (4300), 380 (sh, 1200). EA: Calcd (%) for $C_{20}H_{20}F_6FeN_{10}O_9S_2$: C 30.86; H 2.59; N 17.99. Found: C 30.88, H 2.62, N 18.13.

Computational Details. Geometry optimization calculations for the cations of **2** and **3** were performed with the coordinates obtained from the X-ray crystallographic structure determination. Unrestricted DFT calculations using the *ORCA* program (Ver. 3.0.1, 3.0.2, or 3.0.3) were performed with BP86 (RI approximation) respectively B3LYP (RIJCOSX approximation) functional, and def2-tzvp and def2-tzvp/j basis sets.[59] Solvent effects were considered by invoking the conductor like screening model (COSMO) with acetonitrile as the solvent. TD-DFT calculations were performed with the coordinates obtained from the geometry optimizations (B3LYP functional, RIJCOSX approximation, def2-tzvp and def2-tzvp/j basis sets). 80 excited states were calculated; the maximum dimension of the expansion space in the Davidson procedure (MaxDim) was 800. The p_z character as well as the amount of iron and nitrogen within the HOMO and LUMO result from Mulliken orbital population MO analyses. Mössbauer parameters were computed via unrestricted DFT calculations with the B3LYP functional, def2-tzvp basis set + enlarged CP(PPP) basis set for the Fe atom, dispersion correction D3ZERO, COSMO (acetonitrile).

DOI: 10.1021/jacs.6b00584
J. Am. Chem. Soc. 2016, 138, 7888−7898

Mössbauer isomer shifts were obtained using the correlation formula and parameters reported by Neese et al.[60] X-ray emission spectra were calculated within a one-electron approximation, as described previously.[32] Additional details, as well as a sample input file, are included in the Supporting Information.

■ ASSOCIATED CONTENT

Supporting Information

The Supporting Information is available free of charge on the ACS Publications website at DOI: 10.1021/jacs.6b00584.

Additional figures mentioned in the text; details about DFT calculations and spectroscopic methods. (PDF)
Crystallographic data. (CIF)

■ AUTHOR INFORMATION

Corresponding Authors

*serena.debeer@cec.mpg.de
*franc.meyer@chemie.uni-goettingen.de

Notes

The authors declare no competing financial interest.

■ ACKNOWLEDGMENTS

Experimental support by Jörg Teichgräber and Marie Bergner (both at Georg-August-Universität Göttingen) is gratefully acknowledged. George Cutsail III (MPI-CEC) is gratefully acknowledged for his assistance with X-ray emission measurements. Financial support of this work was provided by the Fonds der Chemischen Industrie (Kekulé scholarship to C.K.), the Deutscher Akademischer Austauschdienst (graduate study scholarship to J.A.R), the Max Planck Society (S.D.) and the DFG (IRTG 1422 "Metal Sites in Biomolecules: Structures, Regulation and Mechanisms"). This work was performed in the framework of the COST action CM 1305 (ECOSTBio). The XES experiments were performed on beamline ID26 at the European Synchrotron Radiation Facility (ESRF), Grenoble, France and beamline C1 at the Cornell High Energy Synchrotron Source (CHESS). We are grateful to Pieter Glatzel at the ESRF and Ken Finkelstein at CHESS for providing technical assistance. CHESS is supported by the NSF and NIH/NIGMS via NSF award DMR-1332208.

■ REFERENCES

(1) Richter-Addo, B.; Legdzins, P. *Metal Nitrosyls*; Oxford University Press: New York, 1992.
(2) Ignarro, J. L. E. *Nitric Oxide, Biology and Pathobiology*; Academic Press: San Diego, CA, 2000.
(3) Zweier, L.; Li, H.; Samouilov, A.; Liu, X. *Nitric Oxide* **2010**, *22*, 83.
(4) Roncaroli, F.; Videla, M.; Slep, L. D.; Olabe, J. A. *Coord. Chem. Rev.* **2007**, *251*, 1903−1930.
(5) Speelman, A. L.; Lehnert, N. *Angew. Chem., Int. Ed.* **2013**, *47*, 12283−12287.
(6) {FeNO}^{x} species are classified according to the Enemark−Feltham notation: Enemark, J. H.; Feltham, R. D. *Coord. Chem. Rev.* **1974**, *13*, 339−406.
(7) Lançon, D.; Kadish, K. M. *J. Am. Chem. Soc.* **1983**, *105*, 5610.
(8) Choi, I. K.; Liu, Y.; Feng, D.; Paeng, K. J.; Ryan, M. D. *Inorg. Chem.* **1991**, *30*, 1832.
(9) Wei, Z.; Ryan, M. D. *Inorg. Chem.* **2010**, *49*, 6948.
(10) Pellegrino, J.; Bari, S. E.; Bikiel, D. E.; Doctorovich, F. *J. Am. Chem. Soc.* **2010**, *132*, 989.
(11) Goodrich, L. E.; Saikat, R.; Alp, E. E.; Zhao, J.; Hu, M. Y.; Lehnert, N. *Inorg. Chem.* **2013**, *52*, 7766.
(12) Hu, B.; Li, J. *Angew. Chem., Int. Ed.* **2015**, *54*, 10579−10582.
(13) Hauser, C.; Glaser, T.; Bill, E.; Weyhermüller, T.; Wieghardt, K. *J. Am. Chem. Soc.* **2000**, *122*, 4352−4365.
(14) Serres, R. G.; Grapperhaus, C. A.; Bothe, E.; Bill, E.; Weyhermüller, T.; Neese, F.; Wieghardt, K. *J. Am. Chem. Soc.* **2004**, *126*, 5138−5153.
(15) Berto, T. C.; Hoffman, M. B.; Murata, Y.; Landenberger, K. B.; Alp, E. E.; Zhao, J.; Lehnert, N. *J. Am. Chem. Soc.* **2011**, *133*, 16714−16717.
(16) Patra, A. K.; Dube, K. S.; Sanders, B. C.; Papaefthymiou, G. C.; Conradie, J.; Ghosh, A.; Harrop, T. C. *Chem. Sci.* **2012**, *3*, 364−369.
(17) Berto, T. C.; Speelman, A. L.; Zheng, S.; Lehnert, N. *Coord. Chem. Rev.* **2013**, *257*, 244−259.
(18) Montenegro, A. C.; Amorebieta, V. T.; Slep, L. D.; Martin, D. F.; Roncaroli, F.; Murgida, D. H.; Bari, S. E.; Olabe, J. A. *Angew. Chem., Int. Ed.* **2009**, *48*, 4213−4216.
(19) Kupper, C.; Schober, A.; Demeshko, S.; Bergner, M.; Meyer, F. *Inorg. Chem.* **2015**, *54*, 3096−3098.
(20) Speelman, A. L.; Lehnert, N. *Acc. Chem. Res.* **2014**, *47*, 1106−1116.
(21) A related {FeNO}^{7} complex of a macrocyclic tetracarbene with smaller ring size showed an irreversible reduction and no oxidation: Anneser, M. R.; Haslinger, S.; Pöthig, A.; Cokoja, M.; Basset, J.-M.; Kühn, F. E. *Inorg. Chem.* **2015**, *54*, 3797−3804.
(22) Meyer, S.; Klawitter, I.; Demeshko, S.; Bill, E.; Meyer, F. *Angew. Chem., Int. Ed.* **2013**, *52*, 901−905.
(23) Pohl, K.; Wieghardt, K. *J. Chem. Soc., Dalton Trans.* **1987**, *1*, 187.
(24) Yoshimura, T. *Inorg. Chim. Acta* **1984**, *83*, 17.
(25) Franz, K. J.; Lippard, S. J. *J. Am. Chem. Soc.* **1999**, *121*, 10504−10512.
(26) Cheng, L.; Powell, D. R.; Khan, M. A.; Richter-Addo, G. B. *Chem. Commun.* **2000**, *23*, 2301−2302.
(27) Holleman, A. F.; Wiberg, E.; Wiberg, N. *Lehrbuch der Anorganischen Chemie*; Walter de Gruyter: Berlin, NY, 1995; p 713.
(28) Rhine, M. A.; Sanders, B. C.; Patra, A. K.; Harrop, T. C. *Inorg. Chem.* **2015**, *54*, 9351−9366.
(29) Lorkovic, I. M.; Ford, P. C. *Inorg. Chem.* **2000**, *39*, 632−633.
(30) Wyllie, G. R. A.; Scheidt, W. R. *Chem. Rev.* **2002**, *102*, 1067−1090.
(31) Hodges, K. D.; Wollmann, R. G.; Kessel, S. L.; Hendrickson, D. N.; Van Derveer, D. G.; Barefield, E. K. *J. Am. Chem. Soc.* **1979**, *101*, 906.
(32) Weber, B.; Käpplinger, I.; Görls, H.; Jäger, E.-G. *Eur. J. Inorg. Chem.* **2005**, *2005*, 2794−2811.
(33) Gütlich, P.; Bill, E.; Trautwein, A. X. *Mössbauer Spectroscopy and Transition Metal Chemistry*; Springer: Heidelberg, 2011.
(34) Ye, S.; Bill, E.; Neese, F. *Inorg. Chem.* **2016**, *55*, 3468−3474.
(35) Tonzetich, Z. J.; Do, L. H.; Lippard, S. J. *J. Am. Chem. Soc.* **2009**, *131*, 7964−7965.
(36) Lindley, B. M.; Swidan, A.; Lobkovsky, E. B.; Wolczanski, P. T.; Adelhardt, M.; Sutter, J.; Meyer, K. *Chem. Sci.* **2015**, *6*, 4730−4736.
(37) Lee, Y.; Mankad, N. P.; Peters, J. C. *Nat. Chem.* **2010**, *2*, 558−565.
(38) Meyer, S.; Krahe, O.; Kupper, C.; Klawitter, I.; Demeshko, S.; Bill, E.; Neese, F.; Meyer, F. *Inorg. Chem.* **2015**, *54*, 9770−9776.
(39) Pollock, C. J.; Delgado-Jaime, M. U.; Atanasov, M.; Neese, F.; DeBeer, S. *J. Am. Chem. Soc.* **2014**, *136*, 9453−9463.
(40) Pollock, C. J.; DeBeer, S. *Acc. Chem. Res.* **2015**, *48*, 2967−2975.
(41) Lee, N.; Petrenko, T.; Bergmann, U.; Neese, F.; DeBeer, S. *J. Am. Chem. Soc.* **2010**, *132*, 9715−9727.
(42) Lu, T.-T.; Weng, T.-C.; Liaw, W.-F. *Angew. Chem., Int. Ed.* **2014**, *53*, 11562−11566.
(43) Pollock, C. J.; Lancaster, K. M.; Finkelstein, K. D.; DeBeer, S. *Inorg. Chem.* **2014**, *53*, 10378−10385.
(44) Römelt, M.; Ye, S.; Neese, F. *Inorg. Chem.* **2009**, *48*, 784−785.
(45) Hunt, A. P.; Lehnert, N. *Acc. Chem. Res.* **2015**, *48*, 2117−2125.
(46) Ye, S.; Price, J. C.; Barr, E. W.; Green, M. T.; Bollinger, J. M.; Krebs, C.; Neese, F. *J. Am. Chem. Soc.* **2010**, *132*, 4739−4751.
(47) Speelman, A. L.; Lehnert, N. *Angew. Chem., Int. Ed.* **2013**, *52*, 12283−12287.

DOI: 10.1021/jacs.6b00584
J. Am. Chem. Soc. 2016, 138, 7888−7898

(48) Berto, T. C.; Hoffman, M. B.; Murata, Y.; Landenberger, K. B.; Alp, E. E.; Zhao, J.; Lehnert, N. *J. Am. Chem. Soc.* **2011**, *133*, 16714−16717.
(49) Delgado-Jaime, M. U.; DeBeer, S. *J. Comput. Chem.* **2012**, *33*, 2180−2185.
(50) Rees, J. A.; Martin-Diaconescu, V.; Kovacs, J. A.; DeBeer, S. *Inorg. Chem.* **2015**, *54*, 6410−6422.
(51) Martin-Diaconescu, V.; Chacón, K. N.; Delgado-Jaime, M. U.; Sokaras, D.; Weng, T.-C.; DeBeer, S.; Blackburn, N. J. *Inorg. Chem.* **2016**, *55*, 3431−3439.
(52) Delgado-Jaime, M.; DeBeer, S.; Bauer, M. *Chem. - Eur. J.* **2013**, *19*, 15888−15897.
(53) Kaljurand, I.; Kütt, A.; Sooväli, L.; Rodima, T.; Mäemets, V.; Leito, I.; Koppel, I. A. *J. Org. Chem.* **2005**, *70*, 1019.
(54) Curley, J. J.; Bergmann, G.; Tilley, T. D. *Dalton Trans.* **2012**, *41*, 192−200.
(55) Lee, W. K.; Liu, B.; Park, C. W.; Shine, H. J.; Guzman-Jimenenz, I. Y.; Whitmire, K. H. *J. Org. Chem.* **1999**, *64*, 9206−9210.
(56) Bill, E. *Mfit*; Max-Planck Institute for Chemical Energy Conversion: Mülheim/Ruhr, Germany.
(57) Stoll, S.; Schweiger, A. *J. Magn. Reson.* **2006**, *178*, 42−55.
(58) Glatzel, P.; Bergmann, U. *Coord. Chem. Rev.* **2005**, *249*, 65−95.
(59) (a) http://libint.valeyev.net. Accessed 16.10.2014. (b) Schaefer, A.; Horn, H.; Ahlrichs, R. *J. Chem. Phys.* **1992**, *97*, 2571. (c) Weigend, F.; Ahlrichs, R. *Phys. Chem. Chem. Phys.* **2005**, *7*, 3297. (d) Neese, F. *Wiley Interdiscip. Rev. Comput. Mol. Sci.* **2012**, *2*, 73−78.
(60) Römelt, M.; Ye, S.; Neese, F. *Inorg. Chem.* **2008**, *48*, 784−785.

DOI: 10.1021/jacs.6b00584
J. Am. Chem. Soc. 2016, 138, 7888−7898